Glass formation in mechanically alloyed Zn-Zr alloy

1993 J. Phys.: Condens. Matter 5 L85

(http://iopscience.iop.org/0953-8984/5/7/002)

J. Phys.: Condens. Matter 5 (1993) L85–L90. Printed in the UK

LETTER TO THE EDITOR

Glass formation in mechanically alloyed Zn–Zr alloy

Zhang Hen†‡, Su Yuchang§, Wu Lijun‡, Wang Lingling‡ and Zhang Bangwei†‡

† CCAST (World Laboratory), PO Box 8730, Beijing 100080, People's Republic of China
‡ Department of Physics, Hunan University, Changsha, Hunan 410012, People's Republic of China
§ Material Test and Research Centre, Hunan University, Changsha, Hunan 410012, People's Republic of China

Received 27 October 1992

Abstract. An amorphous $Zn_{60}Zr_{40}$ alloy was synthesized for the first time by mechanical alloying of pure elemental powders of Zn and Zr using a planetary high-energy ball mill. The structure and thermal behaviour were analysed by x-ray diffraction and differential thermal analysis. The result indicates that the large negative enthalpy of formation of Zn–Zr provides the necessary driving force for solid-state amorphization. In addition, the realization of the amorphization of Zn–Zr shows that Zn is a fast-moving species in host Zr although the ratio of $V_{mp}(Zn)/V(Zr)$ is larger than the critical value of the Zr–TM (3d) system, 0.58. The activation energy of crystallization of the glass is about 3.068 eV.

Since Koch realized the amorphization of Ni–Nb by mechanical alloying (MA) from crystalline elemental nickel and niobium powders [1], this process has been successfully used to amorphize a variety of different alloy systems [2–4]. As a very important group of alloys, TM–TM (TM ≡ transition metal) has attracted considerable interest, and been investigated extensively. These investigations indicated that the glass formation by MA is not restricted to the vicinity of eutectic compositions, but wide amorphization ranges exist in the central part of the phase diagram. From the development of a fine-layered microstructure within the powder particles, it can be found that the transformation is closely related to the solid-state amorphization in binary diffusion couples [5]. In this case, the amorphization would require a layered microstructure to provide a large interface area between the two components, an anomalous fast-diffusion behaviour of one of the elements and, especially, a large negative heat of mixing as the chemical driving force for the diffusion reaction [6]. Based on the literature [7], the occurrence of solid-state amorphization with zirconium as the large atom must satisfy the following: (i) the system must exhibit a negative heat of mixing; (ii) the metal–to–zirconium volume ratio must be less than 0.58. Cu–Zr [6, 8], Ni–Zr [6, 8–14], Co–Zr [6, 8], Fe–Zr [6, 8, 15, 16] and Mn–Zr [6] have been amorphized since they all satisfy the criteria.

Although the 3d transition metals with zirconium have been extensively investigated, the last last-transition element zinc with zirconium has not been

0953-8984/93/070085+06$07.50

investigated yet, even as a binary system; zinc-based alloy is rarely used to prepare amorphous alloy in addition to an Mg–Zn alloy [17]. The purpose of the present work is to investigate the possibility of realizing the amorphization of Zn–Zr by MA. The factors related to the amorphization and thermal behaviour of the alloy were also investigated.

To evaluate the possibility of amorphizing Zn–Zr by MA, we first analyse the chemical driving force which governs a diffusion reaction. The difference in free energy for the solid-state amorphization reaction (SSAR) can be expressed as

$$\Delta G = G_0 - G_a \tag{1}$$

where G_0 is the Gibbs free energy of the high-energy state of an initial crystalline phase after milling; G_a the free energy of the amorphous state, which can be expressed as

$$G_a = \sum_i X_i G_i^a + \Delta H_f^a - T\Delta S_f^a \tag{2}$$

where $\Sigma_i X_i G_i^a$ is a linear combination of the amorphous free energy of pure elements; ΔS_f^a the entropy of formation of the amorphous phase; $T\Delta S_f^a$ is expected to be small because of the lower temperature of SSAR during MA, ΔH_f^a represents the enthalpy formation of the amorphous phase, which can be calculated following the Miedema model [18, 19] since no thermodynamic data exist for amorphous alloys:

$$\Delta H_f = X_A X_B (f_B^A \Delta H_{sol}^{A \text{ in } B} + f_A^B \Delta H_{sol}^{B \text{ in } A}) \tag{3}$$

where $\Delta H_{sol}^{A \text{ in } B}$ is the solution enthalpy of A in B per mole, x the atomic fraction, f_B^A the degree an atom A is surrounded by B atoms, which is given by

$$f_B^A = C_B^S[1 + K(C_A^S C_B^S)^2] \tag{4}$$

where K is an order parameter, which is taken to be 1 or 5 in the case of the absence or presence of short-range chemical order, respectively, and C_B^S is the surface concentration of B atoms.

$$C_B^S = \frac{X_B V_B^{2/3}}{X_A V_A^{2/3} + X_B V_B^{2/3}} \tag{5}$$

with a similar expression and meaning for the parameters C_A^S, f_A^S and $\Delta H_{sol}^{B \text{ in } A}$.

From equations (1)–(3), it is reasonable that a large negative enthalpy can provide the necessary chemical driving force of SSAR. The enthalpy of formation of $Zn_{1-x}Zr_x$ as a function of alloy composition obtained for the amorphous case is shown in figure 1. The ΔH_f for $Zn_{60}Zr_{40}$ is about -37.5 kJ mol^{-1}. This value is not as negative as that of Ni–Zr and Co–Zr, but more negative than that of Cu–Zr, Fe–Zr and Mn–Zr [7, 8]. So the amorphization of Zn–Zr by MA is possible from a thermodynamic viewpoint.

On the other hand, SSAR requires that the system be an asymmetric diffusion couple. The smaller atom in the diffusion couple is the moving species [20–22], which gives a characteristic reaction time for nucleation and growth of the amorphous phase which is shorter than that of the crystalline phase [4, 5, 23]. However, in many cases

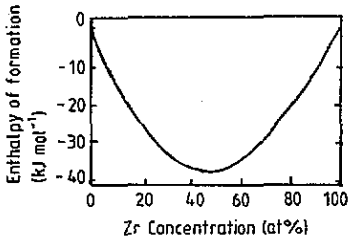

Figure 1. Enthalpy of formation for Zn–Zr alloys as a function of atomic concentration.

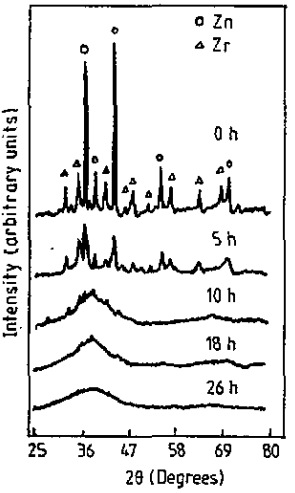

Figure 2. XRD patterns for different milling time of $Zn_{60}Zr_{40}$.

where the interdiffusion coefficient is not known, the metal-to-host volume ratio, which must be less than a certain value, can be used to estimate the diffusivity roughly. In this ratio, the volume of impurity must be corrected according to the Miedema model [24] because of the effect of alloying:

$$\Delta V_{\mathrm{imp}}(\mathrm{A}) = \frac{P_0 V_{\mathrm{A}}^{2/3}(\phi^*_{\mathrm{A}} - \phi^*_{\mathrm{B}})[(n^{\mathrm{A}}_{\mathrm{WS}})^{-1}(n^{\mathrm{B}}_{\mathrm{WS}})^{-1}]}{n(^{\mathrm{A}}_{\mathrm{WS}})^{-1/3} + (n^{\mathrm{B}}_{\mathrm{WS}})^{-1/3}} \tag{6}$$

where V_{A} is the molar volume of pure A, ϕ^* and n_{WS} represent the electronegativity and electron density at the boundary of the Wigner–Seitz cell, and P_0 is a constant.

Using the volume ratio as the dynamic criterion of SSAR is reasonable because in many cases the diffusion coefficient is inversely proportional to the ratio, $V_{\mathrm{imp}}(\mathrm{A})/V(\mathrm{B})$ [25]. The ratio $V_{\mathrm{imp}}(\mathrm{Zn})/V(\mathrm{Zr})$ calculated according to the model is 0.65, which is slightly larger than the critical value of Zr–TM (3d), 0.58 [7]. Nevertheless, since the system Zn–Zr presents a large negative enthalpy of formation, and the ratio of $V_{\mathrm{imp}}(\mathrm{Zn})/V(\mathrm{Zr})$ is near 0.58, it is expected that the amorphization of Zn–Zr can be realized.

Pure elemental powders of Zr (−200 mesh, 99.8%) and Zn (−250 mesh, 99.7%) were mixed to give the desired average composition $Zn_{60}Zr_{40}$ (at.%), and placed in a cylindrical steel vial (40 × 60 mm). The MA was carried out in a planetary high-energy ball-milling machine with a ball-to-powder weight ratio of 10:1 to 15:1. Hardened steel balls 15 mm in diameter were used. At various stages during the milling process samples were analysed by x-ray diffraction (XRD) using a Siemens D-5000 diffractometer with Cu Kα radiation. The thermal behaviour was measured by differential thermal analysis (DTA) using a Rigaku DSC-10A differential scanning calorimeter (DSC) at heating rates of 5, 10, 20, 40 and 80 K min^{-1} under flowing argon.

Two distinct stages were observed during the MA of the Zn and Zr powders. The powders adhered strongly to the surface of the balls and to the walls of the vial forming a hard coating with a rough orange-peel texture during the first couple of

hours. As the milling progressed, this coating fractured off. Further MA caused the alloyed powder to form an agglomerate at one end of the vial. But, this product had the consistency of chalk and could be removed easily. A similar process was also observed during the MA of the Ni–Ti alloy [26] and Ni-based superalloys [27, 28]. The formation of a coating on the ball is advantageous since it presents excessive wear of the balls. But this coating should be kept to a minimum in order to avoid a heterogeneous final product. For the present amorphization process the formation of coating on the ball surface appears to be a desirable feature since it promotes the formation of a multilayer system of alternating Zn and Zr bonds, similar to the thin films obtained by SSAR.

Figure 2 shows a series of XRD patterns taken after 5, 10, 18 and 26 h milling of the $Zn_{60}Zr_{40}$. After five hours of milling, all crystalline Bragg peaks visibly broaden and their intensities decrease. After ten hours of milling, a broad maximum of the amorphous phase appears near $2\theta = 38.41$. The crystalline peaks have vanished completely after 18 h of milling. Apparently, the powders milled for 26 h have transformed to a single amorphous phase completely. The wave number of the broad maximum ($K = 4\lambda \sin\theta/\lambda$) is 2.68 $Å^{-1}$, which is smaller than that of amorphous $Zr_{40}TM_{60}$ (TM = Mn, Cu, Fe) alloys [6, 8], which are 2.71, 2.76 and 2.78 $Å^{-1}$, respectively. The metallic radii of Zn, Mn, Cu and Fe are 1.33, 1.290, 1.275 and 1.241 Å [29], respectively. Therefore, the smaller wave number of $Zn_{60}Zr_{40}$ is attributed to the larger nearest-neighbour distance of Zn–Zr than that of Zr–TM (TM ≡ Mn, Cu, Fe).

Figure 2 indicates the fact that the amorphization takes place mainly between five and eighteen hours of milling and after 18 h, the system is entirely in the amorphous phase. In contrast with the work on $Cu_{60}Ti_{40}$ and $Zn_{60}Ti_{40}$ using the same ball mill [30, 31], we find that the rate of SSAR is nearly as fast as Cu–Ti, but faster than Zn–Ti. From the above analyses of theory and experiment we can conclude that Zn is also an anomalously fast diffuser in the host Zr, although the ratio $V_{imp}(Zn)/V(Zr)$ is larger than 0.58. With the realization of amorphization of Zn–Zr, the dynamic criterion seems to be corrected or extended.

The thermal behaviour and stability of the amorphous powder were measured by DTA. A typical DTA trace for the alloy milled for 26 h at a heating rate of 80 K min^{-1} is shown in figure 3. The MA trace shows a strong exothermic peak from 700 to 900 K and a weak broad exothermic peak from 900 to 1200 K. The crystallization-onset temperature is about 710 K, and the peak temperature is 893 K. The activation energy for crystallization for the first crystallization peak temperature T_c was determined from the DTA measurement at a different rate by the Kissinger method [32]. Analysis of the data in figure 4 gives $\Delta E = 3.068$ eV.

In contrast to $Zr_{40}TM_{60}$ (TM ≡ Cu, Fe, Zr) which were prepared by MA with the same heating rate, 10 K min^{-1}, and which had crystallization temperatures, T_c, 842, 994, and 1001 K, the crystallization temperature T_c of $Zn_{60}Zr_{40}$, 766 K, is very low. If we observe the number of outer electrons (s, d), we may find that the numbers of outer electrons are 7, 8, 11 and 12 for Mn, Fe, Cu and Zn, respectively.

Figure 5 shows that there is a relationship between the crystallization temperature T_c and the average outer-electron concentration (e/a); T_c is inversely proportional to e/a (e/a is given by the weighted means according to the atomic percentage of electrons in the elements). It can be seen that the average valence of the outer electron has a significant effect on T_c: the higher the concentration, the lower T_c. This phenomenon may result from the weakening of bonding with the increase of electron

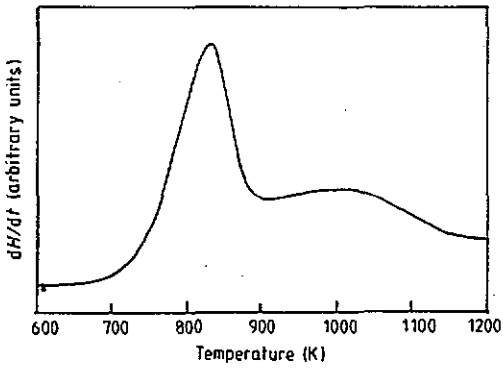

Figure 3. DTA curve for $Zn_{60}Zr_{40}$ milled for 26 h at a heating rate of 80 K min^{-1}.

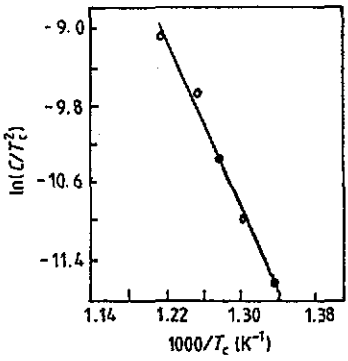

Figure 4. Kissinger plot of the peak of the crystallization exotherm as a function of heating rate C for amorphous $Zn_{60}Zr_{40}$ alloys.

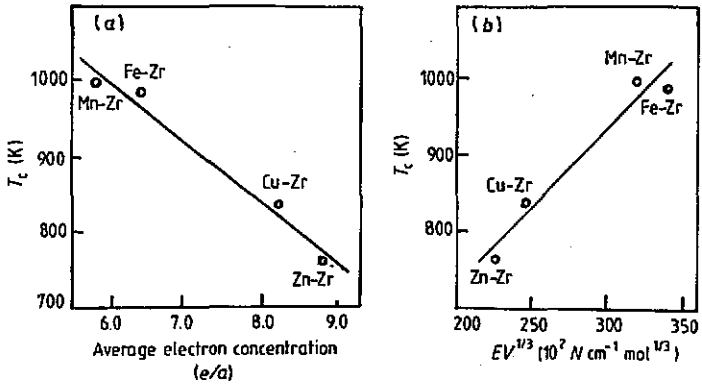

Figure 5. Crystallization temperature T_c versus (*a*) the average outer-electron (s and d) concentration, e/a, (*b*) $EV^{1/3}$, of amorphous $Zr_{40}TM_{60}$ (TM ≡ Zn, Cu, Fe, Mn) alloys.

concentration, whereas the chemical bonding plays a major role in determining the properties of amorphous alloys [33]. The weakening of bonding decreases the attrition of dissimilar atoms and leads to a less stable configuration with decreasing T_c [33]. Therefore, that the highest electron concentration results in the lowest crystallization temperatures for $Zn_{60}Zr_{40}$ is not difficult to understand.

On the other hand, the stability is also related to the parameters $EV^{1/3}$ [34], where E is the elastic modulus, V the atomic volume. In the absence of experimental data, we can estimate the values of $EV^{1/3}$ for the glass using the following expression:

$$EV^{1/3} = X_{Zr}E_{Zr}V_{Zr}^{1/3} + X_{TM}E_{TM}V_{TM}^{1/3}. \tag{7}$$

Introducing the atomic fraction, x, the atomic volume and the elastic modulus of elements from the literature [19, 35] into equation (7), the crystallization temperature T_c versus $EV^{1/3}$ is shown in figure 5(*b*). It shows that T_c is proportional to $EV^{1/3}$, and decreases with $EV^{1/3}$ following the order Fe, Mn, [36, 37] Cu, Zn. Similar phenomena were also observed for Fe–P–C and Cu–Ni–Sn–P systems [37]. The

smallest elastic modulus of Zn and the parameter $EV^{1/3}$ for $Zn_{60}Zr_{40}$ means that the attractive force between dissimilar atoms of the system is not as strong as the other TM–Zr systems. Thus the structure becomes less stable and the stability of the Zn–Zr system is lower than that of the other Zr–TM glasses.

References

[1] Koch C C, Calvin D B, McKamey C G and Scarbrough J O 1983 *Appl. Phys. Lett.* **43** 1017
[2] Weeber A W and Bakker H 1988 *Physica* B **153** 93
[3] Koch C C 1989 *Ann. Rev. Mater. Sci.* **19** 121
[4] Schultz L 1990 *Phil. Mag.* B **61** 453
[5] Schwarz R B and Johnson W L 1983 *Phys. Rev. Lett.* **51** 415
[6] Hellstern E and Schultz L 1987 *Phil. Mag.* B **56** 443
[7] Weeber A W and Bakker H 1987 *Proc. LAM6 (Garmisch-Partekirchen, 1986)* vol 2 (München: Oldenburg) p 221
[8] Hellstern E and Schultz L 1986 *Appl. Phys. Lett.* **48** 124
[9] Weeber A W, van der Meer K, Bakker H, de Boer E R, Thijsse B J and Jongste J F 1986 *J. Phys. F: Met. Phys.* **16** 1897
[10] Gaffet E 1989 *Mater. Sci. Eng.* A **119** 185
[11] Eckert J, Schultz L and Urban K 1991 *J. Non-Cryst. Solids* **130** 273
[12] Weeber A W, Wester A J H, Hang W J and Bakker H 1987 *Physica* B **145** 349
[13] Schultz R, Trudeau M L and von Neste A 1991 *Mater. Sci. Eng.* A **134** 1354
[14] Lee C H, Fukunaga T and Mizutani U 1991 *Mater. Sci. Eng.* A **134** 1334
[15] Hellstern E and Schultz L 1988 *J. Appl. Phys.* **63** 1408
[16] Hellstern E and Schultz L 1986 *Appl. Phys. Lett.* **49** 1163
[17] Calka A and Radlinski A P 1989 *Mater. Sci. Eng.* A **118** 131
[18] Miedema A R, de châtel P F and Boer F R 1980 *Physica* B **100** 1
[19] Niessen A K, Boer F R, Bown R, de châtel P F, Matters C W and Miedema A R 1983 *CALPHAD* **7** 15
[20] Cheng Y T, Johnson W L and Nicholet M A 1985 *Appl. Phys. Lett.* **54** 800
[21] Schroder H, Samwer K and Koster V 1985 *Phys. Rev. Lett.* **54** 197
[22] Barbour J C, Sairs F W and Mager J W 1985 *Phys. Rev.* B **32** 1363
[23] Yech X L, Samwer K and Johnson W L 1983 *Appl. Phys. Lett.* **42** 242
[24] Miedema A R and Niessen A K 1982 *Physica* B **114** 367
[25] Bakker H 1985 *J. Less-Common Met.* **105** 129
[26] Schwarz R B, Petrich R R and Saw C K 1985 *J. Non-Cryst. Solids* **76** 281
[27] Benjamin J S and Bamford M S 1977 *Metall. Trans.* A **8** 1301
[28] Gilman P S and Benjamin J S 1983 *Ann. Rev. Mater. Sci.* **13** 279
[29] Smithells C J and Brandes E A 1976 *Metals Reference Book* (London: Butterworth) p 100
[30] Zhang H and Naugle D G 1992 *Appl. Phys. Lett.* **60** 2738
[31] Zhang H, Su Y C and Wang L L 1992 *Phys. Rev.* B submitted
[32] Kissinger H E 1957 *Ann. Chem.* **29** 1762
[33] Chen H S 1974 *Acta Metall.* **22** 1505
[34] Naka M, Tomizama S, Masumoto T and Watanabe T 1976 *Proc. 2nd Int. Conf. on Rapidly Quenched Metals* ed N J Grant and B C Giessen (Cambridge, MA: MIT) p 273
[35] Brandes E A 1983 *Smithell's Metals Reference Book* (London: Butterworth) pp 18–2
[36] Naka M 1980 *J. Non-Cryst. Solids* **41** 71
[37] Zhang H, Zhang B C and Tan Z S 1992 *Phil. Mag.* B **66** 63